Multi-Band Time of Arrival Estimation for Long Term Evolution (LTE) Signals

M. Noschese[†], F. Babich[†], *Senior Member, IEEE*, M. Comisso[†], *Member, IEEE*, and C. Marshall[§]
[†]Department of Engineering and Architecture, University of Trieste, Via A. Valerio 10, Trieste, Italy
[§]u-blox UK Ltd., 42-48 London Road, Reigate, Surrey, United Kingdom
E-mail: [†]{matteo.noschese@phd.,babich@,mcomisso@}units.it, [§]chris.marshall@u-blox.com

***Abstract*—This paper presents a method for estimating the Time of Arrival (ToA) of Long Term Evolution (LTE) signals received on multiple separate transmission bands by the same Base Station (BS) mast. By exploiting the overall bandwidth occupied by the different signals and the correlation between the corresponding channel impulse responses, a higher precision is achieved with respect to the usually adopted single-band approach whenever the time-correlation among the bands is sufficiently high. The ToA estimation is carried out by generalizing the Space-Alternating Generalized Expectation-maximization (SAGE) algorithm to the multi-band context, proving that the availability of multiple bands provides a reduced standard deviation for the estimated ToA, with a limited increase of the computational cost. The main analyzed issue consists in the management of the asynchrony between transmitters belonging to distinct cellular operators, which is addressed by developing a suitable method to combine the contributions provided by the different bands. The method is validated by simulations in dual- and tri-band scenarios, and is further applied to real dual-band signals measured through a portable setup and experimentally acquired from an LTE BS mast covering multiple cells.**

***Index Terms*—ToA estimation, OFDM, LTE, ranging, SAGE, multi-band.**

I. Introduction

The use of Global Navigation Satellite Systems (GNSSs) for positioning purposes has massively surged over the past decade, following the popularity of location-aware technologies among end-users. Localization-related services are in fact widely employed, ranging from military applications to fleet management, navigation, and entertaining, while GNSS-enabled modules have become affordable and are thus found in the majority of the commercially available mobile devices. However, the accuracy of the position estimated via GNSS is often subject to many impairments that can negatively impact on the quality of the location service, or may even completely disrupt it. Indoor, subterranean, and urban canyon environments can indeed degrade the reception of the positioning signal, until the possible failure of the estimation process. Furthermore, adding a dedicated GNSS-enabled module to a device increases its complexity, leading, in turn, to higher production costs and increased power consumption. These drawbacks are strongly undesirable on user equipments.

Alternative methods able to provide an accurate positioning for land-based systems become hence necessary. These methods usually rely on the estimation of a number of wave parameters for each propagation path, such as its complex amplitude, Time of Arrival (ToA), Doppler shift, and Angle of Arrival (AoA). Various ranging and positioning algorithms have been developed for this purpose, with a specific focus on ToA-based solutions. Direct Line-of-Sight (LoS) ToA estimation and positioning methods in single and multipath scenarios have been in fact widely explored in the literature [1]–[9]. The developed solutions include the Expectation-Maximization (EM) technique [1]–[3], the Super-Resolution Algorithm (SRA) [4], the Estimation of Signal Parameters via Rotational Invariance Techniques (ESPRIT) [5], [6], and the Space-Alternating Generalized EM (SAGE) algorithm [7]–[9].

Within this context, Orthogonal Frequency Division Multiplexing (OFDM) systems present interesting intrinsic properties regarding the estimation of the wave parameters. Besides, many OFDM-based communication technologies, such as Wireless Fidelity (WiFi) and 4G-Long Term Evolution (LTE), are very widespread, thus the design of reliable localization methods exploiting the OFDM properties is an issue of considerable interest [10]–[12]. In WiFi and LTE scenarios, the wireless propagation environment is characterized by multipath, therefore appropriate signal processing techniques are needed to discriminate the LoS path from the non-LoS ones [13]. To this aim, several approaches have been specifically modified to address the ToA evaluation problem in LTE cellular systems, thus considering the achievable precision bounds [14]–[19], and proposing novel methods based on ESPRIT [20], [21], SAGE [22], [23], Frequency Domain Phase (FDP) offset [24], and opportunistic exploitation of reference signals [25].

Among the mentioned techniques, the SAGE algorithm stands out for its versatility and good performance in different propagation environments. Firstly introduced as an extension of EM, SAGE is a reduced complexity method for the evaluation of the Maximum Likelihood (ML) estimator. More precisely, in SAGE, the multi-dimensional ML estimation process is subdivided into a certain number of smaller problems to jointly evaluate the desired parameters in an iterative way. The conventional scenario for the application of SAGE refers to a signal spanning a unique frequency band. However, it is well known that the achievable accuracy is directly related to the bandwidth of the signal [14]. Hence, during DownLink (DL) operations, it may be interesting to acquire multiple signals from the same Base Station (BS), if available, and subsequently combine them to improve the precision of the estimation. In LTE systems, in fact, multiple transmitters can be allocated on the same physical BS mast

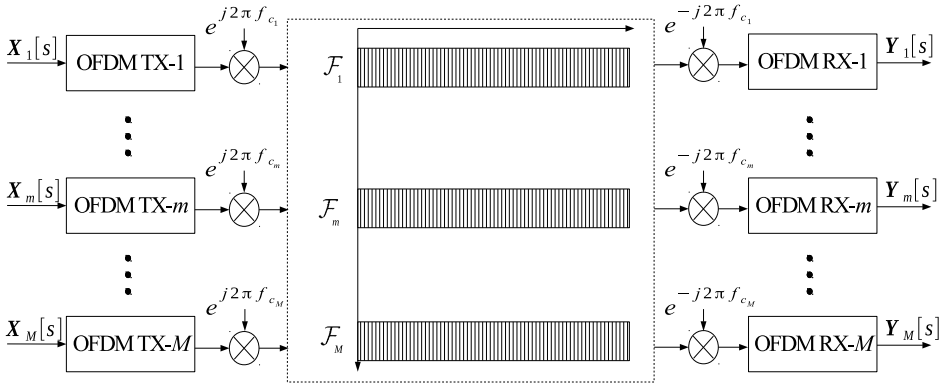

Fig. 1. Multi-band OFDM system ($\mathbf{X}_m[s]$/$\mathbf{Y}_m[s]$: s-th symbol transmitted/received by the m-th subsystem, $\mathcal{F}_m$: set of subcarriers employed by the m-th subsystem, f_{c_m}: m-th carrier frequency).

in order to decrease the deployment cost and improve the network coverage. The DL acquisition can be hence carried out by opportunistically exploiting the Cell-specific Reference Signals (CRSs) transmitted free-to-air by different co-located operators, without the need of increasing the complexity of the Mobile Terminal (MT) or of adopting multiple Subscriber Identity Module (SIM) cards. In general, however, the signals coming from multiple transmitters are not synchronized, thus the capability of combining all the measured data to obtain a more precise estimation requires the evaluation of the time difference between the bands.

This paper specifically addresses this issue by developing a SAGE-based solution that exploits multiple LTE signals simultaneously received on distinct transmission bands. To this aim, a multi-band OFDM signal model is formally developed to account for the complex amplitudes, delays, Doppler shifts, and AoAs of the different multipath components, as well as for the Carrier Frequency Offsets (CFOs) and the Local Oscillator Phase (LOP) shifts of the different subsystems. Moving from this model, an evolution of SAGE for the multi-band context is derived and implemented in Matlab to evaluate the ToA estimation performance in various propagation environments. Moreover, to check the suitability of the conceived solution for real scenarios, the developed method is finally applied to experimental LTE data measured by a portable setup in the city of Monfalcone (Italy), which are acquired from a cellular BS mast carrying multiple transmitters. The main analyzed topic consists in the design of a novel strategy to opportunistically combine the free-to-air CRSs provided by transmitters belonging to different cellular operators. In particular, with respect to [23], the here proposed work presents a more complete signal model, develops a technique to manage the asynchrony between the co-located transmitters, numerically validates the results also in tri-band contexts, and provides experimental results to test the algorithm in real urban scenarios. Besides, with respect to [7]–[9], the presented paper designs a multi-band extension of SAGE, designs a method to account for the synchronization between the clocks of the different LTE DL subsystems, and provides measured values obtained by a real testbed for the most common dual-band case.

The paper is organized as follows. Section II introduces the multi-band OFDM system and the LTE DL signal. Section III presents the proposed multi-band ToA estimation method. Section IV discusses the numerical and experimental results. Finally, Section V summarizes the main conclusions.

Notation. Throughout the paper the following notation is used: $(\cdot)^T$ denotes the transpose operator; '$*$' denotes the convolution operation; '$\otimes$' denotes the element-by-element matrix product; $\mathbb{0}_{R\times C}$ denotes the $R \times C$ null matrix; j denotes the imaginary unit; $\mathrm{Re}(\cdot)$ and $\mathrm{Im}(\cdot)$ denote the real and imaginary parts, respectively; $\delta_{i,k}$ denotes the Kronecker delta ($\delta_{i,k} = 1$ if $i = k$, $\delta_{i,k} = 0$ otherwise); $||\cdot||^2$ denotes the squared norm; $\lfloor\cdot\rfloor$ denotes the floor function; $\delta(\cdot)$ denotes the Dirac delta function; and $\mathrm{E}[\,\cdot\,]$ denotes the expectation operator.

II. Signal Model

A. Multi-band OFDM System

The modeled multi-band OFDM system is reported in Fig. 1. It operates by transmitting the modulated symbols on multiple bands in a parallel way. Since the bands are assumed to be allocated to different operators, the symbols are considered in general different from band to band. The multi-band system is hence organized as the union of $M \geq 1$ non-overlapping single-band OFDM subsystems, where the band available to the generic m-th one ($m = 1, \ldots, M$) is characterized by a carrier frequency f_{c_m} and is in turn subdivided into a certain number of single-carrier narrowband channels. The nonidealities of each subsystem, such as the CFO and the LOP shift, are not reported in Fig. 1, since, for tractability reasons, they will be subsequently included in the Channel Impulse Response (CIR) referred to that subsystem. From a conceptual point of view, different numbers of subcarriers might be considered for each subsystem. However, since, in the LTE standard, the number of subcarriers is one of the mandatory parameters, all subsystems are assumed to have the same number K of subcarriers. Besides, defining as T_s the duration of an OFDM symbol and adopting the conventional OFDM structure, the single-band subcarriers result spaced by a frequency $\Delta f = 1/T_\mathrm{s}$ identical for all subsystems.

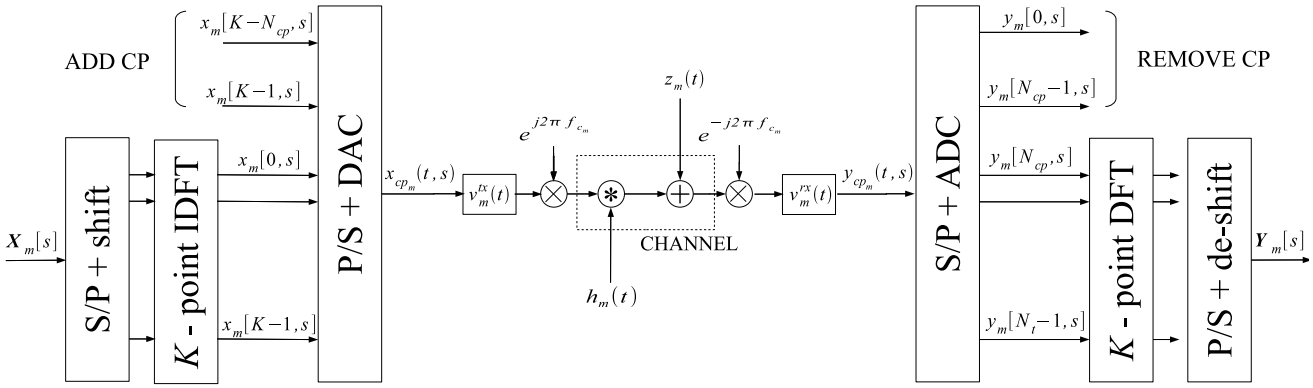

Fig. 2. Generic m-th OFDM subsystem ($x_m[n,s]/y_m[n,s]$: discrete-time transmitted/received signal for the s-th symbol, $x_{\mathrm{cp}_m}(t,s)/y_{\mathrm{cp}_m}(t,s)$: continuous-time transmitted/received signal with CP for the s-th symbol, $h_m(t)$: CIR, $\upsilon_m^{\mathrm{tx/rx}}(t)$: RF transmission/reception filter, $z_m(t)$: AWGN and ICI).

The set of subcarriers employed by the m-th subsystem can be hence expressed as:

$$\mathcal{F}_m = \{f_{mk} \colon k \in \mathcal{K}\}, \quad m = 1, \ldots, M, \tag{1}$$

where $f_{mk} = f_{\mathrm{c}_m} + k\Delta f$ is its k-th frequency and $\mathcal{K} = \{-K/2, \ldots, K/2-1\}$ is the set of the corresponding indexes. Using (1), the total set of subcarriers, having $N = MK$ elements, may be then defined as:

$$\mathcal{F} = \bigcup_{m=1}^{M} \mathcal{F}_m = \{f_q \colon q = 1, \ldots, N\}. \tag{2}$$

Note that, using this general formulation, the frequency spacing between two adjacent subcarriers is no longer equal to Δf in all cases. Yet, for $q = 1, \ldots, N-1$, $f_{q+1} - f_q$ remains identical to Δf just if f_{q+1} and f_q belong to the same band. Moreover, observe that the multi-band OFDM system is organized so that $\max(\mathcal{F}_m) \leq \min(\mathcal{F}_{m+1})$ for $m = 1, \ldots, M-1$, thus the bands are increasingly ordered.

The structure of the m-th single-band subsystem is shown in Fig. 2. Defining the set $\mathcal{S}_m$ of all the OFDM symbols transmitted by this subsystem, consider, for a subcarrier index $k \in \mathcal{K}$ and a symbol $s \in \mathcal{S}_m$, the complex value $X_m[k,s]$ taken from the constellation of a digital modulation. Accordingly, the s-th OFDM symbol to be transmitted can be represented as:

$$\mathbf{X}_m[s] = \left[X_m\left[-\frac{K}{2}, s\right], \ldots, X_m\left[\frac{K}{2}-1, s\right] \right]^T. \tag{3}$$

The corresponding OFDM signal at time t can be hence defined as:

$$x_m(t,s) = \sum_{k \in \mathcal{K}} g(t) X_m[k,s] e^{j2\pi k \Delta f \cdot t}, \quad t \in [0, T_{\mathrm{s}}[, \tag{4}$$

where $g(t)$ is the shaping impulse, which is identified by an ideal rectangle of amplitude 1 and duration T_{s} [26]. The discrete-time signal $x_m[n,s]$, sampled with a period $T = T_{\mathrm{s}}/K$, can then be written for $s \in \mathcal{S}_m$ as:

$$x_m[n,s] = x_m(t,s)\big|_{t=nT} = K \cdot \mathrm{IDFT}\{\tilde{\mathbf{X}}_m[s]\}, \quad n = 0, \ldots, K-1, \tag{5}$$

where IDFT represents the Inverse Discrete Fourier Transform, and:

$$\begin{aligned} \tilde{\mathbf{X}}_m[s] &= \left[\tilde{X}_m\left[-\frac{K}{2}, s\right], \ldots, \tilde{X}_m\left[\frac{K}{2}-1, s\right] \right]^T \\ &= \left[X_m[0,s], \ldots, X_m\left[\frac{K}{2}-1, s\right], \right. \\ &\qquad \left. X_m\left[-\frac{K}{2}, s\right], \ldots, X_m[-1, s] \right]^T, \end{aligned} \tag{6}$$

is obtained from $\mathbf{X}_m[s]$ with the left and right halves swapped. A Cyclic Prefix (CP) is subsequently added to $x_m[n,s]$ by repeating the N_{cp} tail samples of $x_m[n,s]$ before the sequence, in order to enable the subsequent operation of circular convolution. Therefore, defining $N_{\mathrm{t}} = K + N_{\mathrm{cp}}$, the sequence generated by the s-th symbol may be represented as:

$$x_{\mathrm{cp}_m}[n,s] = \begin{cases} x_m[K - N_{\mathrm{cp}} + n, s] & n = 0, \ldots, N_{\mathrm{cp}} - 1 \\ x_m[n - N_{\mathrm{cp}}, s] & n = N_{\mathrm{cp}}, \ldots, N_{\mathrm{t}} - 1 \end{cases} \tag{7}$$

which, after Digital-to-Analog Conversion (DAC) at sampling time T, provides the continuous-time transmitted signal $x_{\mathrm{cp}_m}(t,s)$. This signal then travels through the m-th RadioFrequency (RF) transmission filter, having impulse response $\upsilon_m^{\mathrm{tx}}(t)$, and subsequently, through the up-conversion module, operating at carrier frequency f_{c_m}.

After transmission, the OFDM signal experiences the effects of the propagation environment. For an L_m-path stationary channel, these two elements can be included in the CIR:

$$\begin{aligned} h_m(t) &= \sum_{l=1}^{L_m} \alpha_{m,l} \delta(t - \tau_{m,l}) c(\phi_{m,l}) e^{j\left[2\pi\left(f_{m,l}^{\mathrm{D}} + f_m^{\mathrm{O}}\right)t + \phi_m^{\mathrm{O}}\right]} \\ &= \sum_{l=1}^{L_m} \alpha_{m,l}^{\mathrm{E}} \delta(t - \tau_{m,l}) e^{j2\pi f_{m,l}^{\mathrm{E}} t}, \end{aligned} \tag{8}$$

where, with reference to the m-th subsystem and the l-th path, $\alpha_{m,l}$, $\tau_{m,l}$, $c(\phi_{m,l})$, and $f_{m,l}^{\mathrm{D}}$ denote, respectively, the complex amplitude, the delay, the receiving antenna gain at the AoA $\phi_{m,l}$, and the Doppler frequency shift; f_m^{O} and ϕ_m^{O} represent, respectively, the CFO and the LOP shift between the m-th transmitter and the MT; while $\alpha_{m,l}^{\mathrm{E}} = \alpha_{m,l} c(\phi_{m,l}) e^{j\phi_m^{\mathrm{O}}}$

and $f_{m,l}^{\mathrm{E}} = f_{m,l}^{\mathrm{D}} + f_m^{\mathrm{O}}$ will be from now on referred to as the equivalent complex amplitude and the Doppler-CFO shift, respectively.

Remark 1: For each subsystem, $h_m(t)$ in (8) is formulated considering the delays organized in increasing order, i.e., $\tau_{m,1} < \tau_{m,2} < ... < \tau_{m,L_m}$, thus $\tau_{m,1}$ represents the delay corresponding to the direct path referred to that subsystem. In this context, a basic assumption is necessary to obtain advantages from the adoption of a multi-band approach for ToA estimation purposes. This assumption, which can be formalized as $\tau_{1,1} \cong \tau_{2,1} \cong ... \cong \tau_{M,1} \cong \tau_1$, is identified by the reasonable consistency of the ToAs experienced by the M subsystems when the transmitters of the different operators referred to the same cell are co-located at the same BS mast. Otherwise, no convergence towards a common value would be possible, since the physical problem would not have a unique solution. Note that also the rest of the channel parameters, that is, $\alpha_{m,l}^{\mathrm{E}}$, $f_{m,l}^{\mathrm{E}}$ for $l = 1, ..., L_m$, $m = 1, ..., M$, and $\tau_{m,l}$ for $l = 2, ..., L_m$, $m = 1, ..., M$, will be evaluated during the evolution of the proposed algorithm, but, for them (including the delays not referred to the direct path), no assumptions are required. Hence, these latter parameters can be completely different among the M subsystems without affecting the meaningfulness of the formulated problem. □

According to the Reviewer's request, in the revised paper we have extended *Remark 1* to clarify that, during the evolution of the proposed algorithm, all the three sets of parameters $\alpha_{m,l}^{\mathrm{E}}$, $\tau_{m,l}$, and $f_{m,l}^{\mathrm{E}}$ for $l = 1, ..., L_m$ and $m = 1, ..., M$ require evaluation, even if the final aim is to obtain estimates for $\tau_{1,1}, ..., \tau_{M,1}$.

According to the described channel model, the s-th signal received by the m-th subsystem can be represented as:

$$y_{\mathrm{cp}_m}(t,s) = \left[v_m^{\mathrm{tx}}(t) * h_m(t) * x_{\mathrm{cp}_m}(t,s) + z_m(t)\right] * v_m^{\mathrm{tx}}(t), \quad (9)$$

where $v_m^{\mathrm{rx}}(t)$ denotes the impulse response of the m-th RF receiving filter, while $z_m(t)$ accounts for the Additive White Gaussian Noise (AWGN) and for the Inter-Carrier Interference (ICI). By sampling $y_{\mathrm{cp}_m}(t,s)$ with a period T and removing the CP one obtains the discrete-time signal $y_m[n,s]$.

Remark 2: The ICI due to CFOs, Doppler shifts, and Sampling Frequency Offsets (SFOs) can be modeled as a Gaussian random process by invoking the central limit theorem when K is sufficiently large [27], [28]. For this reason, the process $z_m(t)$ resulting from the sum of AWGN and ICI is from now on assumed Gaussian. □

The subsequent application of the DFT operator to the sampled signal $y_m[n,s]$ provides, for $k \in \mathcal{K}$ and $s \in \mathcal{S}_m$, the OFDM-demodulated signal:

$$\begin{aligned} Y_m[k,s] &= \mathrm{DFT}\left\{y_m[n,s]\right\} \\ &= K \cdot \Upsilon_m[k] H_m[k,s] \tilde{X}_m[k,s] + \tilde{z}_m[k], \end{aligned} \quad (10)$$

where $\Upsilon_m[k] = \mathrm{DFT}\left\{v_m^{\mathrm{tx}}(t) * v_m^{\mathrm{rx}}(t)\,|_{t=nT}\right\}$, $\tilde{z}_m[k] = \mathrm{DFT}\left\{z_m(t) * v_m^{\mathrm{rx}}(t)\,|_{t=nT}\right\}$, and $H_m[k,s]$ is the Channel Frequency Response (CFR). Hence, the s-th received OFDM symbol can be expressed as:

$$\mathbf{Y}_m[s] = \left[Y_m\left[-\frac{K}{2}, s\right], \ldots, Y_m\left[\frac{K}{2} - 1, s\right]\right]^T. \quad (11)$$

The estimation of the CFR may be obtained by the Least-Square (LS) approach using (3), (6), and (11) as [29]:

$$\hat{H}_m[k,s] \approx \frac{Y_m[k,s]}{\Upsilon_m[k]\tilde{X}_m[k,s]}, \quad k \in \mathcal{K}, s \in \mathcal{S}_m, \quad (12)$$

which jointly includes the effects of the propagation channel (complex amplitudes, delays, AoAs, Doppler shifts) and of the subsystem nonidealities (CFO, LOP shift, SFO).

Remark 3: Concerning (12), it is worth to observe that it contains the effects of the transmitting and receiving filters. In general, the usage of RF filters in LTE is not mandatory, but optional [30], thus the term $\Upsilon_m[k]$ might be even absent. In the opposite case, the typical choice consists in the adoption of linear-phase filters, which introduce an additional constant delay over all paths that might be assimilated to the lack of synchrony between transmitter and receiver. This implies that, from the point of view of the ToA estimation problem, a tapped-delay-line channel model can be still assumed. □

B. LTE DL Signal

The above defined multi-band system can be more specifically referred to the LTE DL physical layer [31]. In the LTE standard, the smallest resource unit, corresponding to a single subcarrier of an OFDM symbol, is called Resource Element (RE). Different REs are grouped into Resource Blocks (RBs), each consisting of $N_{\mathrm{sc}}^{\mathrm{RB}} = 12$ adjacent subcarriers spaced by $\Delta f = 15$ kHz and having the duration of one slot, corresponding to 0.5 ms. Each slot is composed of $N_{\mathrm{symb}}^{\mathrm{DL}} = 7$ consecutive OFDM symbols, and each symbol consists of $N_{\mathrm{sc}} = N_{\mathrm{sc}}^{\mathrm{RB}} N_{\mathrm{RB}}^{\mathrm{DL}}$ subcarriers, where $N_{\mathrm{RB}}^{\mathrm{DL}}$ denotes the number of RBs per slot. Two slots generate a subframe, and 10 subframes generate a radio frame. Hence, an LTE frame consists of 20 slots and has a duration of 10 ms.

The LTE standard includes a DL signal specifically designed for ranging applications, called Positioning Reference Signal (PRS). The PRS allows the acquisition of multiple simultaneous user location measurements based on radio access information. Unfortunately, network operators generally avoid transmitting the PRS to reserve more bandwidth for the user data. Hence, this work realistically considers the use of the CRS for the purpose of ToA estimation, since this signal, being essential for authentication and connectivity, is surely made available by any network operator.

The CRS is designed to allow the channel estimation and the coherent demodulation at the receiver, and is always transmitted free-to-air by the BS. For this reason, it can be also opportunistically exploited for positioning purposes [32]. In particular, the CRS is defined as a Quadrature Phase Shift Keying (QPSK)-modulated Gold sequence of length 31, and is mapped onto the REs using a diamond pattern. It is transmitted twice per slot in the first and fifth symbol. The CRS pilot tones are mapped to one subcarrier every six: as such, the number of

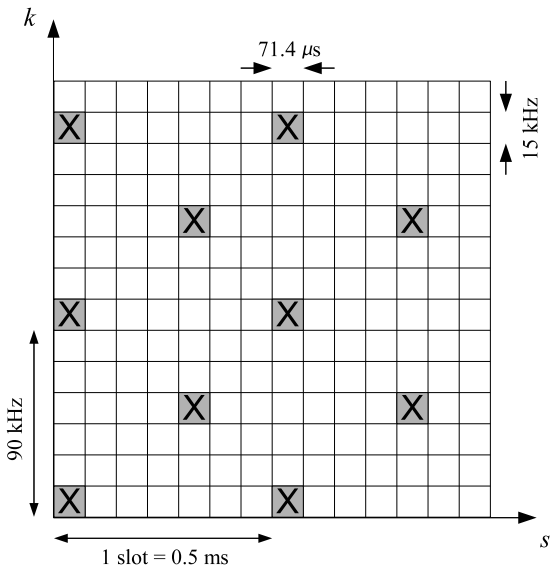

Fig. 3. Possible mapping of the CRS pilot tones (shaded squares) onto REs for the single antenna port configuration [31].

transmitted (and hence observable) CRS tones is $N_{\rm o} = N_{\rm sc}/6$, and the spacing between them is $\Delta f_{\rm o} = 6\Delta f = 90$ kHz. The LTE standard specifies the mapping of the CRS to the REs relying on the Physical Cell ID (PCI), whose value can range between 0 and 503. Six distinct CRS mappings are possible, different by a frequency index shift $\mathrm{PCI} \pmod 6$. If a configuration with multiple antenna ports is used, the CRS is transmitted with different mappings over each port to avoid overlapping. Fig. 3 shows an example of CRS when a single antenna port is used, while Table I lists the possible bandwidth configurations for the LTE DL signals.

These settings, which are applied to the multi-band OFDM system defined in Subsection II-A, allow the identification of a realistic benchmark for the testing of the multi-band ToA estimation method that will be introduced in the next section.

III. Multi-Band ToA Estimation

The explanation of the proposed approach is organized in two parts. The first part illustrates the functionalities of the single-band SAGE algorithm, by focusing the characterization on the m-th subsystem in adherence to the adopted signal model. This part represents a reformulation of the existing analyses, whose aim is to provide a basic description, in terms of notation and mathematical derivations, fundamental to subsequently understand the issues addressed in the multi-band case. The second part indeed uses this formal description to present the developed multi-band ToA estimation strategy, which combines the contributions provided by the different available bands, and manages the problems related to the asynchrony between transmitters belonging to different network operators. The first part is addressed in the following subsection, while the second part is presented in Subsection III-B.

Bandwidth [MHz]	**1.4**	**3.0**	**5.0**	**10.0**	**15.0**	**20.0**
$N_{\rm RB}^{\rm DL}$	6	15	25	50	75	100
$N_{\rm sc} = 12N_{\rm RB}^{\rm DL}$	72	180	300	600	900	1200
$N_{\rm o} = N_{\rm sc}/6$	12	30	50	100	150	200

TABLE I
LTE DL bandwidth configurations [31].

A. Single-band SAGE

The SAGE algorithm is a reduced-complexity extension of the iterative EM technique [1]–[3], which is developed by subdividing the ML maximization problem into a certain number of less complex one-dimensional subproblems. To summarize the basic functionalities of SAGE, let first define the vector $\boldsymbol{\theta}_{m,l} = [\mathrm{Re}(\alpha_{m,l}^{\rm E}), \mathrm{Im}(\alpha_{m,l}^{\rm E}), \tau_{m,l}, \phi_{m,l}, f_{m,l}^{\rm E}]$, which represents the set of parameters of interest for the l-th path and the m-th subsystem. According to the L_m-paths channel model in (8), the entire set of parameters that have to be estimated for the m-th subsystem is $\boldsymbol{\theta}_m = [\boldsymbol{\theta}_{m,1}, \ldots, \boldsymbol{\theta}_{m,L_m}]$, which contains $5L_m$ elements. Let $\mathcal{K}_{\rm o} \subseteq \mathcal{K}$ be the subset of indexes corresponding to the observable subcarriers (i.e., those allocated to the CRS), and $\mathcal{S}_{m_{\rm o}} \subseteq \mathcal{S}_m$ be the subset of not encrypted symbols observable during the CFR sampling from the m-th subsystem. For these two subsets, the CFR LS estimation $\hat{H}_m[k,s]$, which represents the SAGE input data, can be obtained by (12). Using these input data, the ML Estimate (MLE) of $\boldsymbol{\theta}_m$ should be determined by solving the multi-dimensional ML problem, which, unfortunately, is computationally prohibitive because of the large dimension of the searching space and cannot rely on closed-form solutions. For these reasons, the suboptimal approach adopted by the SAGE algorithm results specifically suitable. More precisely, SAGE is based upon the distinction between the complete data, which are unobservable, and the incomplete but observable ones. In particular, considering the L_m-path channel, the actual incomplete observable CFR for the k-th subcarrier and the s-th symbol can be written as:

$$H_m[k,s;\boldsymbol{\theta}_m] = \sum_{l=1}^{L_m} H_{m,l}[k,s;\boldsymbol{\theta}_{m,l}], \quad k \in \mathcal{K}_{\rm o}, s \in \mathcal{S}_{m_{\rm o}}, \quad (13)$$

where the actual complete unobservable data for the l-th path can be expressed as:

$$H_{m,l}[k,s;\boldsymbol{\theta}_{m,l}] = \alpha_{m,l}^{\rm E} c(\phi_{m,l}) e^{j2\pi(f_{m,l}^{\rm E} t_s - f_{mk}\tau_{m,l})}, \quad (14)$$

in which t_s is the instant of transmission of the s-th symbol. These L_m unobservable contributions must be estimated relying on the observable ones $H_m[k,s;\boldsymbol{\theta}_m]$. This is the basic principle of SAGE, which moves from an estimate $\hat{L}_m$ of the number of paths, obtained through the Minimum Description Length (MDL) algorithm [4], to then iteratively update the estimation of the required parameters adopting two basic steps: the Expectation (E) and the Maximization (M). The operations carried out during these two steps can be described as follows [7].

E-step. The E-step updates the estimation $\hat{H}_{m,l}[k,s]$ of the complete unobservable data for one path by exploiting the input data $\hat{H}_m[k,s]$ and a previous estimation $\hat{\boldsymbol{\theta}}_m$ of $\boldsymbol{\theta}_m$. Since, at the first iteration, not all the elements of $\hat{\boldsymbol{\theta}}_m$ are available, a serial interference cancellation approach is adopted. This provides, for iteration $i=1$, the estimation:

$$\hat{H}^1_{m,l}[k,s] = \hat{H}_m[k,s] - \sum_{l'=1}^{l-1} H_{m,l'}[k,s;\hat{\boldsymbol{\theta}}^1_{m,l'}]. \quad (15)$$

For the subsequent iterations, a parallel interference cancellation approach is instead used, thus obtaining, for iteration $i \geq 2$, the estimation:

$$\hat{H}^i_{m,l}[k,s] = \hat{H}_m[k,s] - \sum_{\substack{l'=1 \\ l' \neq l}}^{\hat{L}_m} H_{m,l'}[k,s;\hat{\boldsymbol{\theta}}^{i-1}_{m,l'}]. \quad (16)$$

M-step. The M-step sequentially updates the estimation of the parameters for one path by exploiting the complete data provided by the E-step and the previous estimate of the parameters themselves. More precisely, at iteration $i \geq 1$, the delay, the AoA, and the Doppler-CFO shift are updated, respectively, by:

$$\hat{\tau}^i_{m,l} = \underset{\tau_{m,l}}{\operatorname{argmax}} \left\{ \left| \zeta\left(\tau_{m,l}, \hat{\phi}^{i-1}_{m,l}, \hat{f}^{\mathrm{E}^{i-1}}_{m,l}; \hat{H}^i_{m,l}[k,s]\right) \right| \right\}, \quad (17a)$$

$$\hat{\phi}^i_{m,l} = \underset{\phi_{m,l}}{\operatorname{argmax}} \left\{ \left| \zeta\left(\tau^i_{m,l}, \phi_{m,l}, \hat{f}^{\mathrm{E}^{i-1}}_{m,l}; \hat{H}^i_{m,l}[k,s]\right) \right| \right\}, \quad (17b)$$

$$\hat{f}^{\mathrm{E}^i}_{m,l} = \underset{f^{\mathrm{E}}_{m,l}}{\operatorname{argmax}} \left\{ \left| \zeta\left(\tau^i_{m,l}, \hat{\phi}^i_{m,l}, f^{\mathrm{E}}_{m,l}; \hat{H}^i_{m,l}[k,s]\right) \right| \right\}, \quad (17c)$$

where the correlation function is defined as [8]:

$$\zeta\left(\tau_{m,l}, \phi_{m,l}, f^{\mathrm{E}}_{m,l}; \hat{H}^i_{m,l}[k,s]\right) = c(\phi_{m,l}) \cdot \sum_{k=1}^{K} \hat{H}^i_{m,l}[k,s] e^{j2\pi\left(f_{mk}+f^{\mathrm{E}}_{m,l}\right)\tau_{m,l}}. \quad (18)$$

The equivalent complex amplitude is then updated as:

$$\hat{\alpha}^{\mathrm{E}^i}_{m,l} = \frac{\zeta\left(\hat{\tau}^i_{m,l}, \hat{\phi}^i_{m,l}, \hat{f}^{\mathrm{E}^i}_{m,l}; \hat{H}^i_{m,l}[k,s]\right)}{K_{\mathrm{o}} S_{\mathrm{o}} ||c(\hat{\phi}^i_{m,l})||^2}, \quad (19)$$

where K_{o} and S_{o} are the number of elements of the sets $\mathcal{K}_{\mathrm{o}}$ and $\mathcal{S}_{m_{\mathrm{o}}}$, respectively. Note that, since the symbol duration T_{s} is the same for all subsystems, all sets $\mathcal{S}_{1_{\mathrm{o}}}, \ldots, \mathcal{S}_{M_{\mathrm{o}}}$ are characterized by an identical number of elements, even if each set $\mathcal{S}_{m_{\mathrm{o}}}$ may contain different individual symbols.

At the generic iteration $i \geq 1$, the steps E and M are executed for $\hat{L}_m$ times to obtain the estimation $\hat{\boldsymbol{\theta}}^i_m$ of the whole set of parameters referred to the m-th subsystem. The algorithm is stopped when the convergence is reached for the delay, the AoA, and the Doppler-CFO shift, considering all the estimated paths. More precisely, the algorithm is terminated when all the following $3\hat{L}_m$ conditions are satisfied:

$$\left| \hat{\tau}^i_{m,l} - \hat{\tau}^{i-1}_{m,l} \right| < \bar{\tau}, \;\; l = 1, \ldots, \hat{L}_m, \quad (20a)$$

$$\left| \hat{\phi}^i_{m,l} - \hat{\phi}^{i-1}_{m,l} \right| < \bar{\phi}, \;\; l = 1, \ldots, \hat{L}_m, \quad (20b)$$

$$\left| \hat{f}^{\mathrm{E}^i}_{m,l} - \hat{f}^{\mathrm{E}^{i-1}}_{m,l} \right| < \bar{f}^{\,\mathrm{E}}, \;\; l = 1, \ldots, \hat{L}_m, \quad (20c)$$

in which $\bar{\tau}$, $\bar{\phi}$, and $\bar{f}^{\,\mathrm{E}}$ are properly selected thresholds for the delay, the AoA, and the Doppler-CFO shift, respectively. Once the convergence is reached, $\hat{\tau}_{m,1}$ denotes the single-band ToA estimation provided by the m-th subsystem.

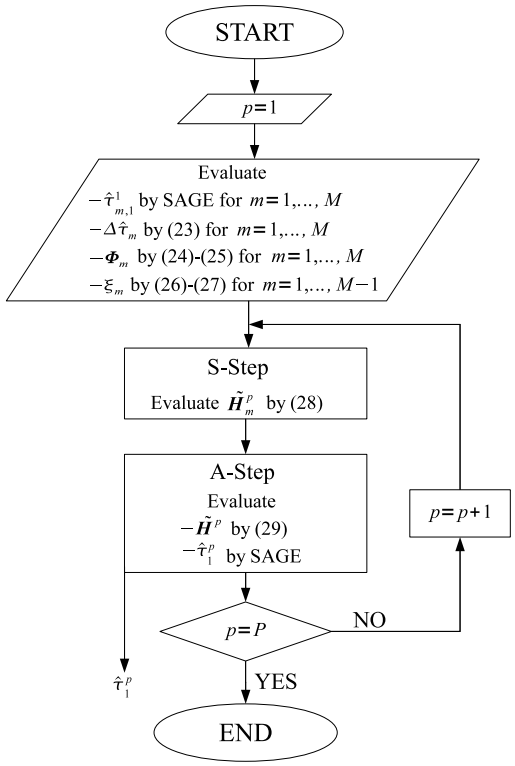

Fig. 4. Multi-band ToA estimation algorithm ove P subsets of consecutive observable OFDM symbols.

B. Multi-band Estimation

The basic reason for moving from a single to a multi-band approach is to employ the information gathered from the overall occupied bandwidth, with the aim of improving the precision of the achieved ToA estimation. This possibility is more attractive when sufficiently close bands are considered, and hence highly correlated CIRs are available. The occurrence of this event represents a not unusual situation, since adjacent bands, belonging to the same portion of the LTE DL spectrum, are commonly allocated to different operators [33], whose transceivers usually share the same BS mast. This implies that, additionally, the BS transmitters of different operators referred to a given cell result co-located. To exploit and manage this scenario, the multi-band ToA estimation algorithm reported in Fig. 4 is here proposed.

For operating on the different bands, the set $\mathcal{S}_{m_\text{o}}$ of all the symbols observable from the m-th subsystem is firstly partitioned into P subsets as:

$$\mathcal{S}_{m_\text{o}} = \bigcup_{p=1,\ldots,P} \mathcal{S}^p_{m_\text{o}}, \quad m = 1, \ldots, M, \tag{21}$$

where each subset $\mathcal{S}^p_{m_\text{o}}$ contains an identical number $\sigma_\text{o} = S_\text{o}/P$ of contiguous elements. This partition enables to consider, for $m=1,\ldots,M$ and $p=1,\ldots,P$, the $K_\text{o} \times \sigma_\text{o}$ matrix:

$$\hat{\mathbf{H}}^p_m = \left[\hat{H}^p_m[k,s]\right], \ \ k \in \mathcal{K}_\text{o}, s \in \mathcal{S}^p_{m_\text{o}}, \tag{22}$$

containing the samples corresponding to the σ_o consecutive OFDM symbols of the p-th subset referred to the m-th subsystem. This operation is carried out for two main reasons: the control of the dimension of the SAGE input data to avoid computational problems due to the usage of too large matrices, and the possibility to update the position information at periodic time intervals.

For initialization purposes, the single-band SAGE is applied to each subset of samples $\hat{\mathbf{H}}^1_m$ for $m = 1,\ldots,M$, so as to obtain, from the first M partitions, M estimations of the delay $\hat{\tau}^1_{1,1},\ldots,\hat{\tau}^1_{M,1}$. Therefore, by selecting, without loss of generality, the time base of the first subsystem as the reference one, the M time shifts that initialize the multi-band ToA estimation process can be expressed as:

$$\Delta\hat{\tau}_m = \hat{\tau}^1_{m,1} - \hat{\tau}^1_{1,1}, \quad m = 1,\ldots,M. \tag{23}$$

Once the initialization is completed, an additional elaboration is carried out to manage the synchronization issue. This issue is addressed by introducing proper shift matrices, which are used to compensate the estimated difference between the clock of the m-th subsystem and that of the reference one. In particular, the generic m-th shift matrix can be defined as:

$$\mathbf{\Phi}^m = \left[e^{-j\phi^m_{k,s}}\right], \tag{24}$$

where, for $k = 1,\ldots,K_\text{o}$, $s = 1,\ldots,\sigma_\text{o}$, and $m = 1,\ldots,M$, the single phase shift is defined as:

$$\phi^m_{k,s} = 2\pi\Delta\hat{\tau}_m \left[k\Delta f_\text{o} + (1-\delta_{m,1})\min(\mathcal{F}_m)\right]. \tag{25}$$

This latter quantity has the objective of compensating the effect of the asynchrony between the clocks of the reference subsystem and of the m-th one for its k-th subcarrier (first term in (25)) and for its entire band (second term in (25)). Since, in general, the M bands are not contiguous, a proper number of null subcarriers can be suitably inserted between them, so as to allow the joining of all the compensated input samples of the p-th subset into an unique complete sample matrix. To this aim, one can define, for $m=1,\ldots,M-1$, the frequency gap between the m-th and the $(m+1)$-th band as:

$$\Delta f_m = \min(\mathcal{F}_{m+1}) - \max(\mathcal{F}_m), \tag{26}$$

which provides the corresponding number of null subcarriers:

$$\xi_m = \left\lfloor \frac{\Delta f_m}{\Delta f_\text{o}} \right\rfloor. \tag{27}$$

Now that all the basic operational quantities have been derived, the multi-band ToA estimation can evolve by performing, for each partition, two basic steps: the Shift (S) and the Aggregation (A). These two steps can be described as follows.

S-step. The S-step manages the synchronization between the clocks of the different subsystems by using the shift matrices in (24)-(25) to obtain the M matrices of the CFR shifted samples for the p-th partition as:

$$\tilde{\mathbf{H}}^p_m = \hat{\mathbf{H}}^p_m \otimes \mathbf{\Phi}^m, \ \ m = 1,\ldots,M. \tag{28}$$

A-Step. The A-step generates the joint sample matrix $\tilde{\mathbf{H}}^p$ for the p-th partition, by inserting, using (26)-(27), the ξ_m null subcarriers between the adjacent bands. This yields:

$$\tilde{\mathbf{H}}^p = \left[\tilde{\mathbf{H}}^p_1 \ \mathbb{0}_{K_\text{o}\times\xi_1} \ \tilde{\mathbf{H}}^p_2 \ldots \tilde{\mathbf{H}}^p_{M-1} \ \mathbb{0}_{K_\text{o}\times\xi_{M-1}} \ \tilde{\mathbf{H}}^p_M\right]. \tag{29}$$

The complete matrix in (29) is given as input to the SAGE algorithm to obtain the estimation $\hat{\tau}^p_1$.

The A- and S-steps are carried out for $p = 1,\ldots,P$ to obtain P estimations of the ToA τ_1 realized by jointly considering all the M available bands. In summary, SAGE is applied M times to initialize the system, and P times to evaluate the P multi-band ToA estimations from the complete shifted sample matrices. Note that these P estimations substantially provide a tracking of the user equipment during the transmission of the S_o symbols. The performance of this tracking is checked in the next section.

IV. Results

The presentation of the results is subdivided in two parts. In the first part, the multi-band ToA estimation is applied to simulated channel data. To this aim, detailed propagation models are implemented by considering the widely adopted COST specifications [34]. In the second part, the developed approach is applied to experimental data acquired through a portable measurement setup. With reference to the CIR in (8), both the simulated and measured results have been derived for $c(\phi) = 1$, $\phi \in [0, 2\pi[$, that is, considering a unity antenna gain. For the ToA estimated at a given Signal to Noise Ratio (SNR) over all the P subsets, the adopted performance figures are: the average value $\hat{\tau}_1 = \mathtt{E}[\hat{\tau}^p_1]$, the standard deviation $\sigma_\tau = \sqrt{\mathtt{E}[(\hat{\tau}^p_1)^2] - \mathtt{E}^2[\hat{\tau}^p_1]}$, and the excursion $\epsilon_\tau = \max(\hat{\tau}^p_1) - \min(\hat{\tau}^p_1)$.

A. Simulations

The simulated data are generated considering single, dual, and tri-band systems, in order to investigate the impact of the

Common		SAGE	
K_o	200	$\bar{\tau}$ [ns]	0.5
P	500	$\bar{\phi}$ [deg]	1
σ_o	20	$\bar{f}^\text{E}$ [Hz]	0.5

TABLE II
ALGORITHM PARAMETERS FOR NUMERICAL SIMULATIONS.

	Scenario 1 (wide delay spread)			Scenario 2 (small delay spread)		
Power profile [dB]	$[0, -2, -10, -20]$			$[0, -4, -8, -12, -16, -20]$		
Delay profile [μs]	$[1.0, 1.2, 1.4, 1.6]$			$[1.0, 1.1, 1.2, 1.3, 1.4, 1.5]$		
Band	$m = 1$	$m = 2$	$m = 3$	$m = 1$	$m = 2$	$m = 3$
f_{c_m} [MHz]	806	816	826	806	816	826
Time offset [μs]	0	0.1	0.2	0	0.1	0.2

TABLE III
COST CHANNEL MODEL CHARACTERISTICS AND SYSTEM PARAMETERS FOR NUMERICAL SIMULATIONS.

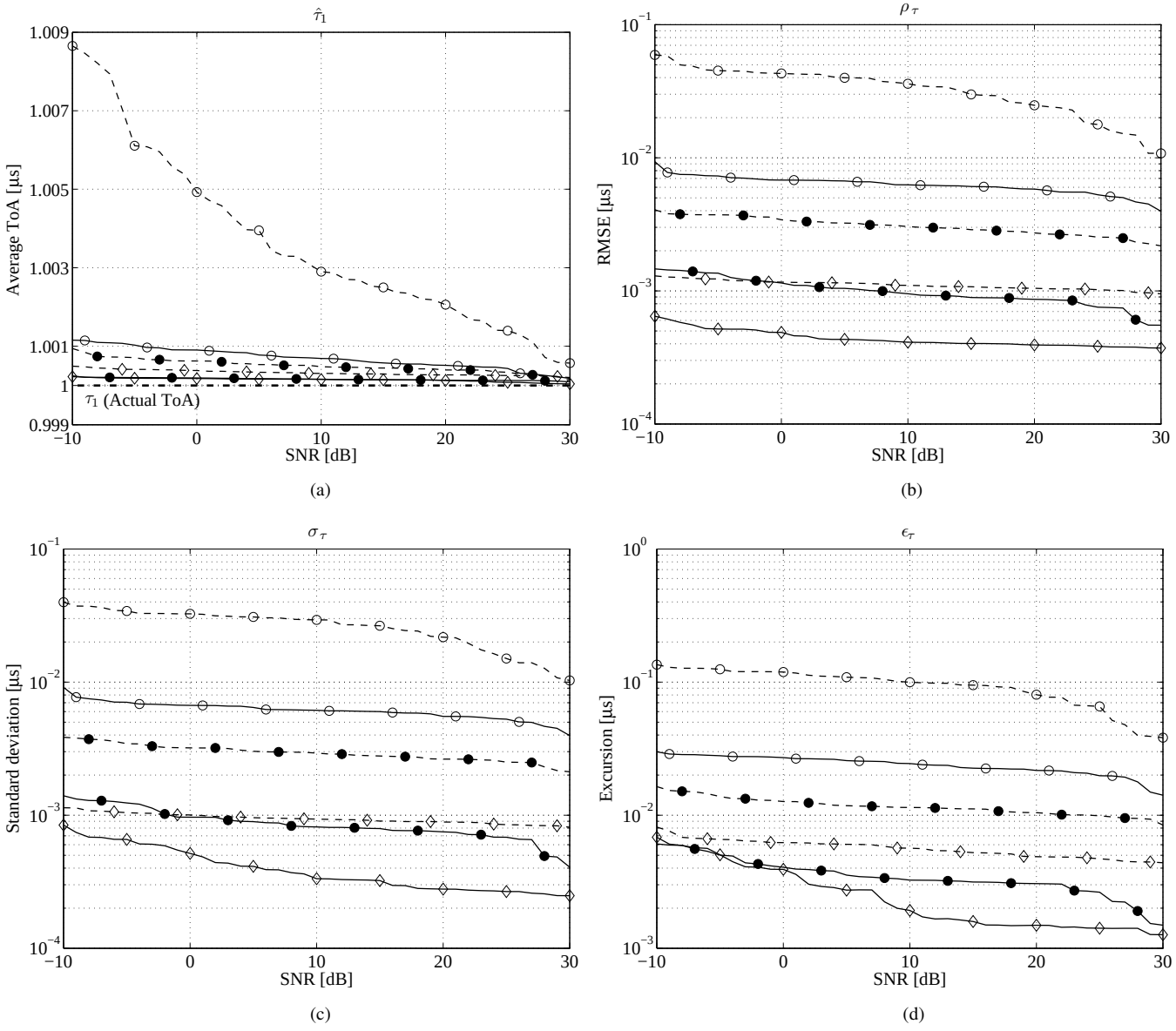

Fig. 5. ToA estimations from numerical simulations.
—○— Scenario 1 (single-band) —●— Scenario 1 (dual-band) —◇— Scenario 1 (tri-band)
- -○- - Scenario 2 (single-band) - -●- - Scenario 2 (dual-band) - -◇- - Scenario 2 (tri-band).

number of bands on the achievable performance. The common system parameters are listed in Table II, while, for the three possibilities, two scenarios are addressed, whose details are reported in Table III. In particular, the single-band system ($M = 1$) uses Band 1, the dual-band system ($M = 2$) uses Bands 1 and 2, while the tri-band system ($M = 3$) uses Bands 1, 2, and 3. Besides, the first scenario is based on the COST207 RA4 channel, which is characterized by a strong second path and a wide delay spread. Instead, the second scenario is based on the COST207 RA6 channel, in which the multiple paths present a smaller delay spread. Each of the three systems is tested in both scenarios, thus obtaining six

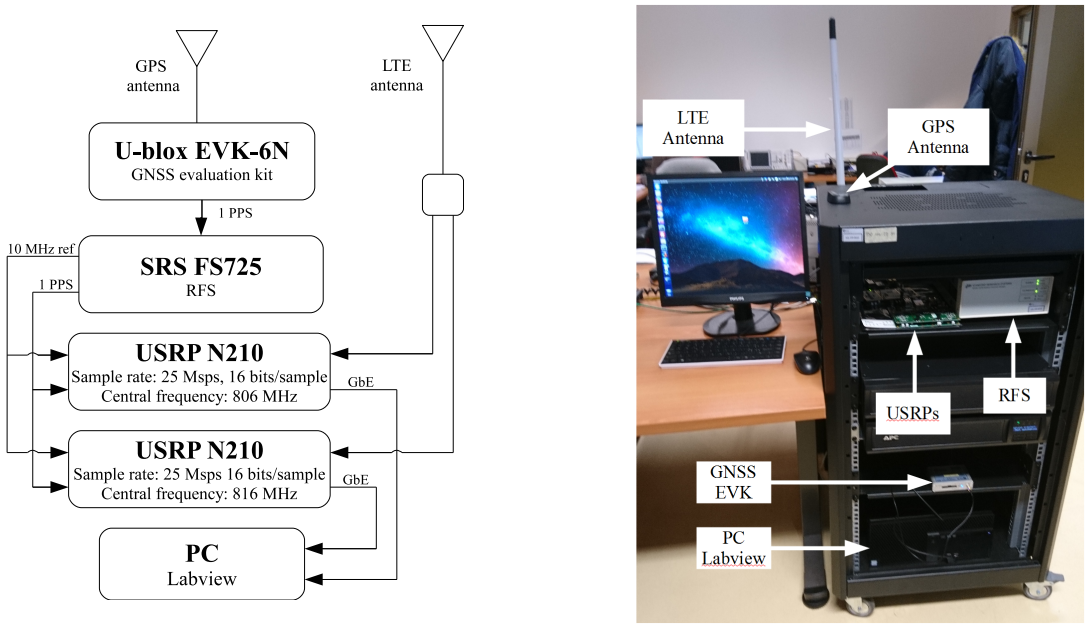

(a) Block scheme

(b) Experimental setup (courtesy of u-blox Ltd. [35])

Fig. 6. Measurement system.

possible cases. Coherently with *Remark 1*, the delay profiles in a given scenario are selected identical for the three bands, and hence the actual ToA τ_1 is the same in each band (i.e., $\tau_1 = \tau_{m,1}$ for $m = 1, \ldots, M$). This however does not imply that the corresponding estimations $\hat{\tau}_{m,1}$ for $m = 1, \ldots, M$ are directly similar, since, as observed in Subsection III-B, the lack of clock synchronization between the transmission bands can lead to different values. For $M \geq 2$, this asynchrony is simulated by introducing constant time offsets (with respect to Band 1), which are estimated by (23) during the evolution of the algorithm. Transmission and reception filters have been assumed absent, coherently with the possibility specified in [30]. The entire framework (propagation environment and multi-band ToA estimation method) is implemented in Matlab and, to simplify the readability of the presented figures, the actual ToA τ_1 has been selected equal to 1 μs for all cases.

The obtained results are shown in Fig. 5, which reports, for each SNR value, the average ToA (Fig. 5(a)), the Root Mean Square Error (RMSE) $\rho_\tau = \mathrm{E}[(\tau_1 - \hat{\tau}_1^p)^2]$ (Fig. 5(b)), the standard deviation (Fig. 5(c)), and the excursion (Fig. 5(d)). Fig. 5(a) shows that, for both scenarios, the multi-band approach outperforms the conventional single-band one, since the dual- and tri-band estimations are increasingly closer to the actual ToA (thick dash-dotted line). This is more evident from Scenario 2, where the single-band estimation presents a large gap with respect to the actual ToA at low-to-mid SNR values. The reason of this behavior is the larger number of paths and the lower delay spread that characterize the second scenario, which cannot be resolved as the bandwidth is limited. The satisfactory performance provided by the multi-band approach is confirmed by the RMSE in Fig. 5(b), which, mainly for Scenario 2, highlights the higher sensitivity of the single-band estimation to the SNR level. Beside the precision, in fact, the multi-band strategy presents a higher robustness against the noise level, becoming capable to operate also in low SNR regimes. This aspect is remarked by Fig. 5(c), which, showing the standard deviation, represents an indicator of the stability of the estimation in static conditions. Finally, the excursion in Fig. 5(d) reveals that also the magnitude of the outliers is reduced when more bands are available.

A global observation of Fig. 5 illustrates that the higher the number of available bands, the better the ToA estimation. More precisely, the transition from one to two bands provides the highest performance gain, while this gain is lower in the transition from two to three bands. From a practical perspective, this characteristic makes of specific interest the dual-band systems, which are the more likely to occur in existing BSs supporting multiple cellular operators.

B. Measurements

According to the observation formulated at the end of the previous subsection, the developed multi-band ToA estimation system has been applied to experimental channel samples acquired from a real dual-band system (i.e., $M = 2$). These samples are obtained using the setup reported in Fig. 6 to collect static measurements from an operating cellular BS. The setup is made up of two Universal Software-defined Radio Peripheral (USRP) platforms N210, which simultaneously measure the DL channels allocated to two network operators transmitting from the same BS mast. A high-precision 10 MHz reference clock generated by a GPS-locked Rubidium Frequency Standard (RFS) is employed for synchronizing the two USRPs. The u-blox EVK-6N GNSS evaluation kit provides the GPS-locked Pulse Per Second (PPS) signal to

	Position 1 (low distance and partial obscuration)		Position 2 (large distance and good visibility)	
	Single-band	Dual-band	Single-band	Dual-band
Average ToA $\hat{\tau}_1$ [μs]	0.087	0.087	0.120	0.120
Standard deviation σ_τ [μs]	0.478	0.195	0.344	0.213
Excursion ϵ_τ [μs]	2.748	0.877	1.568	0.866

TABLE IV
TOA ESTIMATIONS FROM EXPERIMENTAL DATA.

the Rubidium clock. A conventional Personal Computer (PC), connected to the two USRPs through Gigabit-Ethernet (GbE) interfaces, acts as system controller and data recording unit, guaranteeing the coherent sampling between the two USRP devices. Labview is used as data acquisition software for configuration purposes. The data are recorded in a binary format, with a sampling rate of 25 mega-samples per second (Msps) and a 16 bits precision for the real and imaginary part of each sample. The radio waves are received through a wideband LTE antenna coupled with a two-way splitter without adopting specific RF receiving filters. Note that the RFS-based precision clock is adopted to ensure a common time reference for the data acquired through the two USRPs, but is not capable to solve the asynchrony problem between the two monitored bands. As discussed in detail in Subsection III-B, this problem is in fact solved by the proposed algorithm during the S-step using (24), (25), and (28).

The measurements are carried out in the city of Monfalcone (Italy), in an industrial district characterized by low-rise buildings and parking lots separated by wide roads. The considered BS mast is used by two different network operators, with 3 PCIs for each operator arranged in a sectored configuration. The mast transmits on two separate bands, centered around 806 MHz and 816 MHz (LTE band 20), with a 10 MHz transmission bandwidth on both carrier frequencies. The measurements are acquired in different positions around the BS. Among these positions, the reported results are referred to two specific ones, which are representative of two different scenarios (Fig. 7): one characterized by a partial obscuration but a low distance from the mast (Position 1), and another one characterized by a satisfactory visibility but a larger distance from the BS (Position 2). Each measurement trace consists of 500 ms of continuous recording, corresponding to 50 LTE DL frames. The PCIs of the visible cells are inferred from the acquired data by combining the information provided by online cell archives with the CellSearch scan tool [37], [38]. The identified PCIs are 384, 385 and 386 for the 806 MHz band, and 9, 10 and 11 for the 816 MHz band. Since these values are fundamental to correctly extract the CFR by (12), they are further checked by correlating the measured samples with a locally-generated CRS signal for all possible PCIs.

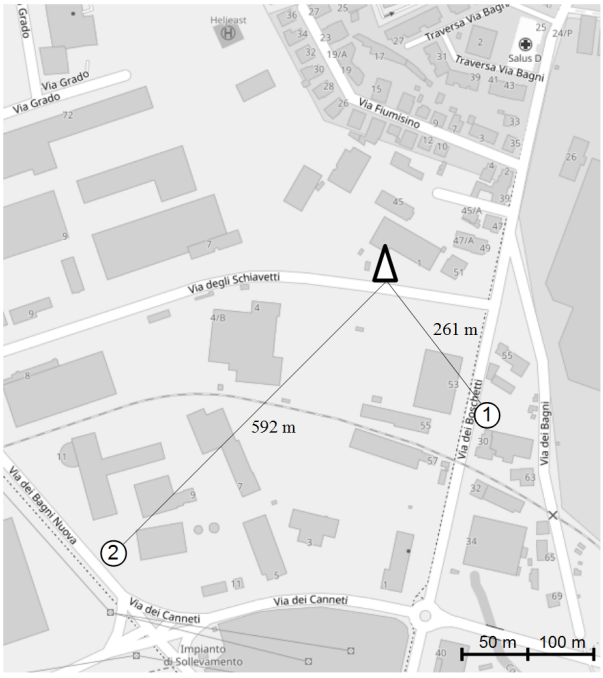

Fig. 7. Map of the considered urban area in the city of Monfalcone (courtesy of OpenStreetMap [36]). The triangle denotes the BS position and the circles identify the measurement positions (Position 1: worse visibility and lower distance from BS, Position 2: better visibility and larger distance from BS).

The results derived from the experimental samples are presented in Table IV, which reports the average ToA, the standard deviation, and the excursion for each considered position. Note that the RMSE is not derived, since the actual ToA is unknown. From the available quantities, one can notice that, in both positions, the σ_τ and ϵ_τ values derived for the dual-band case are lower than those obtained for the single-band one. This reveals that, also using experimental data, the multi-band approach is characterized by a higher robustness. With specific reference to Position 1, the higher ϵ_τ value for the single-band case suggests the existence of some outliers, due to the presence of vegetation partially obscuring the transmitter. The lower ϵ_τ value for the same position but referred to the dual-band case confirms, instead, that these outliers are much reduced when the dual-band approach is employed. Conversely, in Position 2, the propagation environment is characterized by a more clear visibility of the BS, thus the estimated values are less scattered. Anyway, also in this situation, the dual-band algorithm presents a lower standard deviation and a lower excursion. Beside the previously simulated scenarios, these latter results encouragingly confirm, on one hand, the practical advantages that may be achieved when more bands are available, and, on the other hand, that these advantages can be properly exploited by the proposed multi-band ToA estimation approach.

V. Conclusions

A multi-band ToA estimation method for OFDM-based LTE DL systems has been proposed. The method has been conceived by developing a SAGE-based algorithm to exploit the signals incoming from different cellular operators co-located on the same BS mast. The conceived strategy has been validated by simulations and experimental measurements acquired through a portable setup. The multi-band ToA estimations have shown considerable improvements in terms of precision with respect to the conventional single-band approach. In particular, the dual-band experimental results have shown, for the standard deviation and the excursion, improvements in the order of 40% in scenarios characterized by clear BS visibility and in the order of 60% in partially obscured scenarios. Furthermore, it is worth to notice that a really interesting advantage of the presented approach, which involves the sole not encrypted free-to-air CRS signals, is its immediate applicability. In fact, the CRS signals are continuously broadcasted by the BS and their simultaneous transmission from different operators is not required by the proposed algorithm. Besides, no hardware/software modifications are requested at the BS and no additional LTE protocols are necessary to make feasible the multi-band ToA estimation. The increased functionalities are instead entirely at charge of the MT, for which a custom measurement setup has been adopted with the aim of outlining the practical feasibility of the conceived solution.

Acknowledgements

The authors would like to thank Dr. Alessandro Pin, from University of Udine, and Dr. Marco Driusso, from u-blox, for the design and development of the measurement setup.

References

[1] A.P. Dempster, N.M. Laird, and D.B. Rubin, "Maximum likelihood for incomplete data via the EM algorithm," *J. Royal Statistic Soc. Ser. B*, vol. 39, no. 1, pp. 1–38, 1977.

[2] T.K. Moon, "The expectation-maximization algorithm," *IEEE Signal Process. Mag.*, vol. 3, no. 6, pp. 47–60, Nov. 1996.

[3] G. McLachlan and T. Krishnan, *The EM Algorithm and Extensions*. New York: Springer, 1998.

[4] X. Li and K. Pahlavan, "Super-resolution ToA estimation with diversity for indoor geolocation," *IEEE Trans. Wireless Commun.*, vol. 3, no. 1, pp. 224–234, Jan. 2004.

[5] R. Roy and T. Kailath, "ESPRIT - Estimation of signal parameters via rotational invariance techniques," *IEEE Trans. Acoust., Speech, Signal Process.*, vol. 37, no. 7, pp. 984–995, July 1989.

[6] A. Jakobsson, A.L. Swindlehurst, and P. Stoica, "Subspace-based estimation of time delays and Doppler shifts," *IEEE Trans. Signal Process.*, vol. 46, no. 9, pp. 2472–3623, Sept. 1998.

[7] B.H. Fleury, M. Tschudin, R. Heddergott, D. Dahlhaus, and K.I. Pedersen, "Channel parameter estimation in mobile radio environments using the SAGE algorithm," *IEEE J. Sel. Areas Commun.*, vol. 17, no. 3, pp. 434–450, Mar. 1999.

[8] C.C. Chong, D.I. Laurenson, C.M. Tan, S. McLaughlin, M.A. Beach, and A.R. Nix, "Joint detection estimation of directional channel parameters using the 2-D frequency domain SAGE algorithm with serial interference cancellation," in *IEEE ICC*, 2002.

[9] D. Shutin and B.H. Fleury, "Sparse variational bayesian SAGE algorithm with application to the estimation of multipath wireless channels," *IEEE Trans. Signal Process.*, vol. 59, no. 8, pp. 3609–3623, Aug. 2011.

[10] S.A. Golden and S.S. Bateman, "Sensor measurements for Wi-Fi location with emphasis on time-of-arrival ranging," *IEEE Trans. Mobile Comput.*, vol. 6, no. 10, pp. 1185–1198, Oct. 2007.

[11] F. Ricciato, S. Sciancalepore, F. Gringoli, N. Facchi, and G. Boggia, "Position and velocity estimation of a non-cooperative source from asynchronous packet arrival time measurements," *IEEE Trans. Mobile Comput.*, vol. 17, no. 9, pp. 2166–2179, Sept. 2018.

[12] W. Gong and J. Liu, "RoArray: Towards more robust indoor localization using sparse recovery with commodity WiFi," *IEEE Trans. Mobile Comput.*, vol. 18, no. 6, pp. 1380–1391, June 2019.

[13] C.K. Seow and S.Y. Tan, "Non-line-of-sight localization in multipath environments," *IEEE Trans. Mobile Comput.*, vol. 7, no. 5, pp. 647–660, May 2008.

[14] R.K. Martin, C. Yan, H.H. Fan, and C. Rondeau, "Algorithms and bounds for distributed TDOA-based positioning using OFDM signals," *IEEE Trans. Signal Process.*, vol. 59, no. 3, pp. 1255–1268, Mar. 2011.

[15] A. Mallat, S. Gezici, D. Dardari, C. Craeye, and L. Vandendorpe, "Statistics of the MLE and approximate upper and lower bounds - Part I: Application to TOA estimation," *IEEE Trans. Signal Process.*, vol. 62, no. 21, pp. 5663–5676, Nov. 2014.

[16] M. Driusso, M. Comisso, F. Babich, and C. Marshall, "Performance analysis of time of arrival estimation on OFDM signals," *IEEE Signal Process. Lett.*, vol. 22, no. 7, pp. 983–987, July 2015.

[17] K. Shamaei, J. Khalife, and Z.M. Kassas, "Ranging precision analysis of LTE signals," in *IEEE EUSIPCO*, 2017.

[18] K. Shamaei, J. Khalife, and Z.M. Kassas, "Pseudorange and multipath analysis of positioning with LTE secondary synchronization signals," in *IEEE WCNC*, 2018.

[19] Y. Karisan, D. Dardari, S. Gezici, A.A. D'Amico, and U. Mengali, "Range estimation in multicarrier systems in the presence of interference: Performance limits and optimal signal design," *IEEE Trans. Wireless Commun.*, vol. 10, no. 10, pp. 3321–3331, Oct. 2011.

[20] Y. Wang, X. Ma, C. Chen, and X. Guan, "Designing dual-tone radio interferometric positioning systems," *IEEE Trans. Signal Process.*, vol. 63, no. 6, pp. 1351–1365, Mar. 2015.

[21] M. Driusso, C. Marshall, M. Sabathy, F. Knutti, H. Mathis, and F. Babich, "Vehicular position tracking using LTE signals," *IEEE Trans. Veh. Technol.*, vol. 66, no. 2, pp. 3376–3391, Apr. 2017.

[22] W. Wang, T. Jost, C. Gentner, S. Zhang, and A. Dammann, "A semiblind tracking algorithm for joint communication and ranging with OFDM signals," *IEEE Trans. Veh. Technol.*, vol. 65, no. 7, pp. 5237–5250, July 2016.

[23] M. Noschese, F. Babich, M. Comisso, and C. Marshall, "On the performance of SAGE algorithm for ToA estimation in dual-band OFDM systems," in *IEEE PIMRC*, 2018.

[24] Y.-J. Chen, J.-H. Peng, K.-Z. Huang, and X.-R. Gong, "A multipath delay estimation model and algorithm in OFDM systems," in *IEEE ICIST*, 2014.

[25] M. Noschese, F. Babich, M. Comisso, C. Marshall, and M. Driusso, "A low-complexity approach for time of arrival estimation in OFDM systems," in *IEEE ISWCS*, 2017.

[26] J.G. Proakis and M. Salehi, *Digital Communications*. New York: McGraw-Hill Education, 2000.

[27] M. Russell and G.L. Stüber, "Interchannel interference analysis of OFDM in a mobile environment," in *IEEE VTC*, 1995.

[28] M. García and C. Oberli, "Intercarrier interference in OFDM: A general model for transmissions in mobile environments with imperfect synchronization," *EURASIP J. Wireless Commun. Netw.*, vol. 2009, pp. 1–10, Article ID786040.

[29] Y. Liu, Z. Tan, H. Hu, L. Cimini, and G. Li, "Channel estimation for OFDM," *IEEE Commun. Surveys Tut.*, vol. 16, no. 4, pp. 1891–1908, 2014.

[30] *Evolved Universal Terrestrial Radio Access (E-UTRA); Base Station (BS) radio transmission and reception (Rel. 14)*, 3GPP, Apr. 2017.

[31] *Evolved Universal Terrestrial Radio Access (E-UTRA); Physical channels and modulation (Rel. 12)*, 3GPP, Dec. 2015.

[32] A. Dammann, S. Sand, and R. Raulefs, "Signals of opportunity in mobile radio positioning," in *IEEE EUSIPCO*, 2012.

[33] "Ministry of Economic Development - National Plan for Frequency Partitioning." [Online]. Available: https://www.mise.gov.it/index.php/it/comunicazioni/radio/pnrf-piano-nazionale-di-ripartizione-delle-frequenze

[34] M. Patzold, *Mobile Fading Channels*. Hoboken: Wiley, 2002.

[35] "u-blox." [Online]. Available: https://www.u-blox.com/

[36] "OpenStreetMap." [Online]. Available: https://www.openstreetmap.org/

[37] "Cellular coverage and tower map." [Online]. Available: http://www.cellmapper.net

[38] "LTE SDR cell scanner." [Online]. Available: https://github.com/Evrytania/LTE-Cell-Scanner

Matteo Noschese received the B.Sc., M.Sc. and Ph.D. degrees in Communication Engineering from the University of Trieste, Italy, in 2009, 2015, and 2019, respectively. From 2010 to 2015 he worked for MQUADRO as embedded system developer. His research interests include positioning, signal processing, cellular networks, Low Density Parity Check (LDPC) codes, and network protocols.

Fulvio Babich (SM'02) received the doctoral degree, (Laurea), cum laude, in Electrical Engineering, at the University of Trieste, on July 1984. After graduation he was with Telettra at the Research and Development Laboratories, where he was engaged in optical fiber communications. Then he joined Zeltron, where he was a communication system engineer, responsible of the activities within the ESPRIT program. In 1992 he joined the Department of Electrical and Electronic Engineering (DEEI) of the University of Trieste, where he is Professor of Digital Communications and Wireless Networks. Currently, Fulvio Babich is vice-director of the Department of Engineering and Architecture (DIA) and coordinator of the Ph.D. program for Industrial and Information Engineering of the University of Trieste. He is also member of the board of the National Telecommunications and Information Theory Group (GTTI), and was member of the Directive Board of the National Inter-University Consortium for Telecommunications (CNIT). His current research interests are in the field of wireless networks and millimeter-wave communications, where he is involved in channel modeling, multiple access techniques, channel encoding, error control techniques, and cross-layer design.

Massimiliano Comisso (M'09) received the Laurea degree in Electronic Engineering and the Ph.D. degree in Information Engineering from the University of Trieste, Italy. He was with Alcatel, where he worked on DWDM communication systems, and collaborated with Danieli Automation on electromagnetic NDE techniques. Currently, Massimiliano Comisso is an Assistant Professor at the Department of Engineering and Architecture (DIA) of the University of Trieste. He is author/co-author of more than 80 international scientific papers, and serves as referee/TPC member for several IEEE journals and conferences. He has been Best Student Paper Award (BPA) Finalist at GLOBECOM 2006 and received the BPA at CAMAD 2009. His research interests involve distributed wireless networks, millimeter-wave communications, antenna array synthesis, and small antennas.

Chris Marshall received the M.A. degree in natural and electrical sciences from the University of Cambridge, Cambridge, UK, in 1980 and the Ph.D. degree from Imperial College London, London, UK in 1985. In 1980, after his master's studies, he joined Philips Research Laboratories. He pursued and led a variety of research and advanced development activities with Philips in the UK and, from 1991 to 1996, in Germany. He worked on one of the first chipsets for Global System for Mobile Communications (GSM) digital cellular transceivers, and on the air-interface standard IEEE 802.15.4 used for machine-to-machine wireless connectivity systems such as ZigBee. From 2003, he led Philips' creation of software GPS technology and was the Chief Technology Officer of the NXP spin-out Geotate, which was acquired by u-blox UK Ltd., Reigate, UK, in 2009. He is currently creating cellular positioning product technology. Dr. Marshall is a Fellow of the Institution of Engineering and Technology (IET).